

Serveur Académique Lausannois SERVAL [serval.unil.ch](http://serval.unil.ch)

## Author Manuscript

### Faculty of Biology and Medicine Publication

**This paper has been peer-reviewed but does not include the final publisher proof-corrections or journal pagination.**

Published in final edited form as:

**Title:** Light intensity modulates the regulatory network of the shade avoidance response in Arabidopsis.

**Authors:** Hersch M, Lorrain S, de Wit M, Trevisan M, Ljung K, Bergmann S, Fankhauser C

**Journal:** Proceedings of the National Academy of Sciences of the United States of America

**Year:** 2014 Apr 29

**Volume:** 111

**Issue:** 17

**Pages:** 6515-20

**DOI:** 10.1073/pnas.1320355111

In the absence of a copyright statement, users should assume that standard copyright protection applies, unless the article contains an explicit statement to the contrary. In case of doubt, contact the journal publisher to verify the copyright status of an article.

**Classification:** BIOLOGICAL SCIENCES, Systems Biology/Plant Biology

**Title: Light intensity modulates the regulatory network of the shade avoidance response in Arabidopsis**

**Authors:**

Micha Hersch<sup>1, 2, †</sup>, Séverine Lorrain<sup>1, 3, †</sup>, Mieke de Wit<sup>3</sup>, Martine Trevisan<sup>3</sup>, Karin Ljung<sup>4</sup>, Sven Bergmann<sup>1, 2, 5</sup>, Christian Fankhauser<sup>3, 5</sup>

**Author affiliation:**

<sup>1</sup> Swiss Institute for Bioinformatics, CH-1015 Lausanne, Switzerland

<sup>2</sup> Department of Medical Genetics, Faculty of Biology and Medicine, University of Lausanne, CH-1015 Lausanne, Switzerland.

<sup>3</sup> Centre for Integrative Genomics, Faculty of Biology and Medicine, University of Lausanne, CH-1015 Lausanne, Switzerland.

<sup>4</sup> Umeå Plant Science Centre, Department of Forest Genetics and Plant Physiology, Swedish University of Agricultural Sciences, SE-901 83, Umeå, Sweden

<sup>†</sup> authors with equal contribution listed by alphabetical order

<sup>5</sup> **Corresponding authors:**

Christian Fankhauser,

Centre for Integrative Genomics, Faculty of Biology and Medicine, University of Lausanne, CH-1015 Lausanne, Switzerland.

[Christian.Fankhauser@unil.ch](mailto:Christian.Fankhauser@unil.ch), +41.21.692.39.41

**Keywords:**

Shade avoidance, Auxin signaling, Phytochrome Interacting Factor (PIF), regulatory network model.

## **Abstract**

Plants such as *Arabidopsis thaliana* respond to foliar shade and neighbors who may become competitors for light resources by elongation growth to secure access to unfiltered sunlight. Challenges faced during this Shade Avoidance Response (SAR) are different under a light-absorbing canopy and during neighbor detection where light remains abundant. In both situations elongation growth depends on auxin and bHLH class transcription factors of the Phytochrome Interacting Factor (PIF) class. Using a computational modeling approach to study the SAR regulatory network, we identify and experimentally validate a novel role for HFR1 (long Hypocotyl in Far Red 1) a negative regulator of the PIFs. Moreover, we find that during neighbor detection, growth is promoted primarily by the production of auxin. In contrast, in true shade the system operates with less auxin but with an increased sensitivity to the hormonal signal. Our data suggest that this latter signal is less robust, which may reflect a cost-to-robustness trade-off, a system trait long recognized by engineers and forming the basis of information theory.

## **Significance statement (120 words max)**

Plants sense foliar shade and neighbors who may become competitors for light. Shade-sensitive species elongate in response to both situation to enhance access to unfiltered sunlight, which is known as the Shade Avoidance Response (SAR). During neighbor detection plants have access to plenty of light (energy resources) while in true shade light resources are scarce. Our analysis of the molecular mechanisms underlying SAR under these contrasting conditions shows that light intensity balances the production and sensitivity of the growth hormone auxin. In foliar shade the production of auxin is reduced while the downstream sensitivity to the auxin signal is enhanced. This hints at a resource-aware signaling where the strength of the hormonal signal is tuned to the

available resources.

**\body**

## **Introduction**

Being photoautotrophic and inescapably exposed to their environment, plants have developed sophisticated ways to adapt to their surroundings and secure access to light (1). For example, when grown in close proximity to neighboring plants, many species develop elongated stems and smaller leaves, a behavior called the Shade Avoidance Response (SAR) (Fig. 1A) (2). This increases their chance of reaching out to the sunlight above other plants and thus constitutes a competitive advantage (3). Committing additional resources to upward growth is so crucial that it happens at the expense of other functions, such as defense against pest and pathogens (4). An appropriate allocation of resources is vital for the plant, especially during its early and vulnerable developmental stage (5).

The SAR is triggered not only by a reduction in the amount of light but also by specific modifications of its spectrum due to plant properties. Photosynthetic pigments absorb red (R) and blue (B) light, while plants scatter far-red light (FR) leading to a reduction of the R:FR ratio in their vicinity. Under a foliar canopy, access to exploitable light (the Photosynthetically Active Radiation, PAR) is reduced and plants sense both a low level of PAR and a low R:FR ratio. Due to FR scattering, a low R:FR ratio can also occur without a decrease in light resources when a plant is surrounded by non-shading neighbors (potential future competitors for light), a feature termed neighbor detection (2). Both neighbor detection and foliar shade lead to similar growth responses characterized in seedlings by the elongation of the embryonic stem (hypocotyl). However, it remains poorly understood how this can be achieved either in light-limiting conditions (true shade) or when plants retain access to the full solar spectrum (neighbor

detection). In order to investigate how the R:FR ratio is transduced in these two contexts, we analyzed the effect of low R:FR in high versus low PAR using combined computational and biological approaches. As both pathways require the hormone auxin and the transcription factors PIF4 and PIF5 (Phytochrome Interacting Factor), we concentrated our analysis on these regulators of the SAR (6–8), leaving out other regulators such as PIF7, whose role have only been described in one of those conditions (9).

Current knowledge regarding the interplay between PIF4/5 and auxin during the SAR can be summarized into a simplified model shown in Fig. 1B. The R:FR ratio is perceived by the phytochrome B (phyB) photoreceptor that shifts between an inactive (PrB) and active (PfrB) form. The active form interacts with and inactivates the PIFs, which are positive regulators of the SAR. In high R:FR, phyB is active and targets the PIFs for phosphorylation/degradation, thus repressing the activation of the shade-avoidance program (7, 9). In the vicinity of other plants, the low R:FR converts phyB into its inactive form and the PIFs are free to activate gene expression. In particular PIFs modulate the auxin pathway as well as the activation of a negative feedback loop involving the transcription factor HFR1 (10, 11). In low R:FR auxin is quickly produced by the TAA1-YUCCA pathway in the cotyledons (embryonic leaves). It is then transported to the hypocotyl to induce its elongation (12, 13).

We modeled this regulation by a network model and rely on it to generate different hypotheses that were experimentally validated to untangle the interaction between the PIFs and the auxin pathways. This combination of computational modeling with experimental validation lead us to uncover that HFR1 regulates auxin levels independently of PIF4 and PIF5 and that the intensity of the auxin signal and its downstream sensitivity depend on the light intensity, i.e., on the availability of resources.

## Results

### Model assessment

The network model (Fig. 1C) has the R:FR ratio as single input and the hypocotyl elongation as the single output. Molecular activities are represented by nodes that are connected to each other by arrows representing positive or negative effects. The network is modeled by a dynamical system, where the state of each node is determined by the equation in Fig. 1D at steady-state. The corresponding node is set to zero when the activity is null, for example in a mutant (see Material and Methods).

The network model was first tested in one condition, true shade (low R:FR and low PAR). To do so, we determined hypocotyl length of seedlings grown for four days in high R:FR before being transferred to high or low R:FR for four more days. The elongation during these last four days was used as an experimental read-out corresponding to the elongation node of the network model (Fig. S1). This protocol was performed with the wild type (Col) and the following genotypes *pif4pif5*, *hfr1*, a *taa1* allele called *sav3-2*, *hfr1pif4pif5*, *hfr1taa1*, *pif4pif5taa1* (see Material and Methods).

Rather than estimating or optimizing the parameters as it is usually done (14), we sample them from a distribution determined from the biological data. This parameter distribution is used to predict the hypocotyl elongation in a given condition. To evaluate the network model, a leave-one-mutant-out cross-validation procedure was applied, and the mean prediction error was used as the model score. This makes the model evaluation independent from a particular choice of parameters (which are hardly accessible), takes into account the intrinsic variability of the biological data and avoids overfitting (see Material and Methods). This procedure was applied to test the ability of our initial model to predict the elongation of seedlings in response to high or

low R:FR, when trained on all other mutants and the WT elongation data. This analysis showed that the elongation of many mutants was not properly predicted (Fig. 2A), hinting at some weakness in the model.

**HFR1 inhibits auxin production, while PIF4 and PIF5 regulate auxin sensitivity in true shade.**

To increase the prediction accuracy of the model, we tried to add edges to our network. Looking at the elongation data, we noticed that the *hfr1pif4pif5* mutant differs from the *pif4pif5* mutant, a fact that cannot be accounted for from the literature or in our present network, as it assumes that HFR1 acts through PIF4 and PIF5 (10). The best improvements we found was adding a negative edge from HFR1 to auxin or to the YUCs, the simulations being unable to significantly distinguish between both scenarios. This suggests that HFR1 (directly or indirectly) inhibits the production of auxin in a pathway parallel to PIF4 and PIF5 (Fig. 2B).

This new edge significantly increased the network prediction accuracy, however, some mutants were still poorly predicted, especially the *pif4pif5* double mutant (Fig. 2B). In a previous paper, we reported that PIF4 and PIF5 control auxin production but also sensitivity (8). We thus tested whether the model predicted that PIF4 and PIF5 increased auxin sensitivity rather than production or both. As sensitivity cannot be described with the equation of Fig. 1D, we model it as a product between PIF4/5 and auxin activities (see Material and Methods). This link rather than the PIF4/PIF5-YUCs link provided a strong improvement in the prediction accuracy (Fig. 2C and Fig. S2)

Taken together, the results of our network simulation suggest that 1) HFR1 inhibits auxin

production 2) HFR1 also acts independently of PIF4 and PIF5 and 3) PIF4 and PIF5 regulate auxin sensitivity rather than production in low light intensity.

To determine whether the excessive growth of *hfr1* was mediated by an increase in auxin levels we first grew seedlings in the presence of the polar auxin transport inhibitor NPA, which totally suppressed growth (Fig. 3A). We then determined the sensitivity of *hfr1* to the auxin biosynthesis inhibitor L-kynurenine (15). The *hfr1* mutant was less affected by L-kynurenine than the wild type, suggesting that auxin production is up-regulated in *hfr1* (Fig. 3B). This was further established by measuring auxin content, which was higher in *hfr1* than in the wild type (Fig. 3C). To explore how HFR1 regulates auxin content, gene expression quantification using RT-qPCR was performed. *YUC2*, *YUC8* and *YUC9*, which encode rate-limiting enzymes in auxin synthesis downstream of TAA1, were over-expressed in *hfr1* (Fig. 3D and Fig. S3) (16). This is consistent with the finding that auxin levels are also increased in *hfr1taa1* compared to *taa1* (Fig. 3C). The second prediction from our simulations was that HFR1 represses auxin production independently from PIF4 and PIF5. The normal expression of *YUC2*, *YUC8* and *YUC9* in *pif4pif5* and the elevated expression of *YUC* genes in *hfr1pif4pif5* support this hypothesis (Fig. 3D and Fig. S3). The important role played by PIF7 during the shade avoidance prompted us to check whether HFR1 may act by inhibiting this member of the PIF family (9). Expression quantification of *YUC* genes in *pif7*, *hfr1* and the double mutant showed that elevated *YUC* expression levels in *hfr1* depended partially or totally on PIF7 (Fig. S4). Finally, our third prediction - that PIF4 and PIF5 rather act downstream of auxin production - is consistent with our gene expression data (Fig. 3D and Fig. S3). We thus propose that in low light, PIF4 and PIF5 modulate the low R:FR signal through HFR1 inhibition of auxin production and through their effect on auxin sensitivity.

### **Stronger auxin production but weaker sensitivity in neighbor detection than in true shade**

To determine whether the same regulatory network explains the growth response during neighbor detection, we repeated this experimental protocol but in high PAR. The network providing the best predictions was the one where PIFs induce auxin production and do not influence auxin sensitivity (Fig. 4A and Fig. S5). This, along with the best-performing network obtained in true shade conditions, suggests a differential role for PIF4/5 in low and high light intensity in response to low R:FR treatment. This is consistent with our previously published results that PIF4 and PIF5 have a weaker effect on auxin sensitivity in high than in low light intensity (8). To test whether PIF4 and PIF5 have a differential effect on auxin production depending on PAR, we analyzed the sensitivity of *pif4pif5* to yucasin, an inhibitor of YUC enzymes (17), in seedlings grown in high versus low PAR and subjected to low R/FR. Interestingly, *pif4pif5* displayed an increased sensitivity to yucasin only in high PAR, consistent with the hypothesis that PIF4 and PIF5 primarily control YUC-mediated auxin production in this condition (Fig S6).

More generally, the difference between the best-performing network in both conditions hints at a modulation of auxin production versus sensitivity dependent on light intensity. We thus propose that for low R:FR signaling, in low light intensity auxin sensitivity is enhanced, while auxin production is stronger in high light intensity. This would suggest an adaptive signaling depending on the availability of resources. As photosynthesis is less productive in low light, we hypothesized that less auxin would be produced (18, 19). Consequently the SAR would involve lower levels of auxin that would be compensated at least partially by a higher sensitivity.

Supporting our hypothesis, we measured more auxin in the aerial part of the plant in high than in low light intensity (Fig. 4B). Another observation points to elevated auxin levels in high light that involves both TAA1-dependent and independent pathways. In our conditions, the *taa1* mutant

reacted to the low R:FR treatment in high but not in low light intensity, a response that was inhibited by the auxin perception inhibitor PEO-IAA (Fig. S7).

The effect of light intensity on auxin production and sensitivity was further validated by the differential effect of competitive inhibitors (Fig. 4C). On one hand, the auxin biosynthesis inhibitor L-kynurenine was more efficient to inhibit hypocotyl elongation under low than under high light conditions, while the auxin perception inhibitor PEO-IAA was more efficient in high than in low light intensity. This is consistent with more auxin production under high PAR (see also Fig. 4B), while in low PAR auxin sensitivity is enhanced. The mechanisms underlying auxin sensitivity are presumably multifactorial, however, the effect of PEO-IAA suggested a possible role for auxin receptors (Fig. 4C). Our previous ChIP-seq. analysis identified *AFBI*, a gene coding for an auxin receptor, as a potential PIF5 target gene (8). We reasoned that to control auxin sensitivity of hypocotyl growth this gene should be expressed in hypocotyls. We thus analyzed expression of *AFBI* in dissected seedlings grown in high or low PAR and transferred into low R:FR. Interestingly low R:FR led to up-regulation of *AFBI* expression in hypocotyls while in cotyledons this response was marginal (Fig. 4D and Fig. S8). Moreover, low R/FR-mediated *AFBI* expression was significantly stronger when seedlings were grown in low than in high PAR (Fig. 4D). Finally, we showed that in seedlings grown in low PAR, low R/FR-mediated *AFBI* expression largely depended on PIF4 and PIF5 (Fig. 4E).

Collectively, our results indicate that light quantity and thus resource availability determines the amount of auxin produced, in other words the hormonal signal intensity. A strong signal (high auxin level) is more costly and requires more resources, but is likely to be more robust than a cheaper and weaker signal. To verify whether this trade-off prediction is supported by our data, we fitted the data to a noise model that distinguishes the measurement noise from the auxin signal

read-out noise (see Supplemental Information). The latter was indeed significantly reduced in high versus low PAR for Col, (F-test, p-value < 1e-7). This was reproduced in an independent dataset (F-test, p-value < 1e-4) but was not observed in *pif4pif5* and *hfr1pif4pif5* (Fig S9) in line with a putative role of the PIFs in the modulation of the auxin signal intensity.

## Discussion

This work, which integrates modeling and experimental approaches, provides new insights both in terms of biology and methodology. Regarding the methodological aspects, it shows that although the model is very coarse, it can provide novel insights into a biological system, something that has long been argued by the boolean network community (20). However, in contrast to standard boolean networks and their continuous extension (21), our model can make accurate quantitative predictions, which is particularly appropriate for a system with a continuous output such as hypocotyl elongation. The accuracy of the predictions is attributable to the parameter sampling approach that we used. This approach, which is reminiscent of Approximate Bayesian Computation (see Material and Methods), marginalizes over the parameters and seems to extract the global constraints imposed by the network topology, irrespective of particular parameter values. This is why the coarseness of the model, assuming only linear and bilinear activation and inactivation, does not hamper the precision of the predictions.

Regarding the biological aspects, our experimental validations made extensive use of drug treatments. This pharmacological approach allows us to deal with the genetic redundancy at the level of auxin biosynthesis and auxin receptor genes. Moreover, it allowed us to challenge auxin signaling or biosynthesis at specific times, which is otherwise only doable with conditional mutants that are, to our knowledge, unfortunately inexistent. Pharmacological experiments indicated that HFR1 inhibits auxin production (Fig. 3A and B), which was further demonstrated by direct auxin measurements (Fig. 3C). Moreover we show that in the conditions tested here HFR1 acts independently from PIF4 and PIF5 (Fig. 3D). In contrast, HFR1 acts partially but not exclusively through PIF7, as the epistatic relationship between *hfr1* and *pif7* is distinct for the expression of different *YUC* genes (Fig. S4). We propose that the elevated levels of auxin in *hfr1*

are the result of the increased expression of the *YUC* genes in the mutant as it has been reported that over-expression of *YUC1* can rescue the short hypocotyl phenotype of *taa1* in shade (16). Consistent with this idea *hfr1* partially suppresses the shade phenotype of *taa1* (Fig. 2 and Fig. S5).

More globally, our study indicates that the way the low R:FR signal is transduced into auxin signaling pathway depends on the availability of light resources (Fig. 4). Under high light conditions where resources are abundant, plants produce more carbohydrates that may be associated with more auxin production (18, 19). Thus in response to low R:FR a strong auxin signal can be produced. However, in a low light environment, the overall auxin production is weaker (Fig. 4B) and thus signal intensity may be reduced. We propose that to compensate for reduced auxin levels due to a lack of resources in low light conditions, the sensitivity to auxin is enhanced, as if the hypocotyl expecting a lower signal, was “listening” more carefully (Fig. S10). How auxin sensitivity is translated in terms of molecular activity is complex and poorly understood. Auxin is perceived by a co-receptor formed by a member of the TIR1/AFB family and an Aux/IAA protein (22, 23). Here we show that in response to shade *AFB1* is selectively up-regulated in the hypocotyl, which may contribute to enhanced sensitivity of this organ to auxin (Fig. 4D, Fig 4E and Fig. S8). Interestingly, robust *AFB1* up-regulation depends on PIF4 and PIF5 and is greater at low than high PAR (Fig. 4D and E). Moreover, PIF4 and PIF5 directly control the expression of members of the Aux/IAA family (8), which may also contribute to the control of auxin sensitivity. The increased sensitivity to auxin could also be achieved through the brassinosteroids, previously shown to be required for low blue induced shade avoidance (13), and to increase auxin sensitivity (24).

This signal modulation is likely related to the energetic cost of signal transduction, the reduction

of which would be advantageous in conditions of low resources even at the cost of its robustness. The difference between signaling cascades in the context of neighbor detection and canopy shade avoidance may thus depend not only on light signals as such, but also on the internal energy status of the plant. The co-regulation of hormonal signal production and downstream sensitivity to the same hormone has also been described in the case of insulin (25). The present study begs the question of the optimization by the plant of a trade-off between cost and robustness of the signal. This trade-off has long been recognized as fundamental by engineers and its study laid the foundation of information theory to quantify the amount, cost and reliability of information transmission (26). Biological systems also face this trade-off, which was investigated in the case of neural signal transduction (27). Our work on shade avoidance suggests that in plants, hormonal signaling can also be subjected to this trade-off. Interestingly, a recent study involving information theoretic measures on mammalian cells showed that transmitting an information through the amplitude of a signal (as is usually assumed) is not the most robust way (28), thus also hinting that more elaborate modes of signaling should also be envisaged in the study of biological systems.

## Material and Methods

### *Growth conditions*

For determination of hypocotyl length, approx. 40 seeds were plated on 1.6 % agar ½ MS plate on a 180 µm nylon net filter (Millipore). Plates were kept 3 days in the dark and cold before being transferred at 20-21°C in a Percival AR22L incubator (<http://www.percival-scientific.com/products/arabidopsis-chamber>) in constant white light (PAR =110 µmol m<sup>-2</sup> s<sup>-1</sup>, R:FR=12.2 or PAR =30 µmol m<sup>-2</sup> s<sup>-1</sup>, R:FR=13.8). The spectral light composition in the Percival incubator was measured as described in (29). Plates were kept vertically so that seedlings grew along the mesh. After 4 days in high R:FR ratio, plates were transferred into low R:FR conditions (PAR= 110 µmol m<sup>-2</sup> s<sup>-1</sup> supplemented with FR=60 µmol m<sup>-2</sup> s<sup>-1</sup>, R:FR=0.7 or PAR =30 µmol m<sup>-2</sup> s<sup>-1</sup>, R:FR=40 µmol m<sup>-2</sup> s<sup>-1</sup>, R:FR=0.3) or kept in the same conditions as a control for 4 more days. Pictures of the plates were taken at days 04 and 08. Hypocotyl length was measured using the ImageJ software (<http://rsbweb.nih.gov/ij/>).

Further information on the biological material and methods is available in the supplement.

### *Computational method*

A detailed account of the computational method is provided in the Supplemental Information. In summary, the network is modeled using the following Ordinary Differential Equation (ODE) system:

$$\dot{x}_i = s_i + a_{ji}x_j - k_i x_i - d_{ji}x_j x_i,$$

where  $x_i$  is the positive molecular activity of node  $i$ ,  $s_i$  a constant activation term,  $k_i$  a constant inactivation rate, and  $a_{ji}$  and  $d_{ji}$  are the activation and inactivation effects of node  $j$  on node  $i$ . To model sensitivity, a bilinear activation term  $a_{ijk}x_j x_k$  is added to this equation. The network output, (elongation) is gated by a sigmoidal function of the form  $y = \beta(1 + \exp(-x + \beta/2))^{-1}$ , of amplitude  $\beta$ .

The network parameter vector  $\theta$  thus contains one (effective) parameter per node ( $s_i/k_i$ ), one parameter per edge and  $\beta$ . To train the network, a parameter sampling approach is taken rather than optimizing the parameters. This is done by sampling the parameter space such that the distribution of network outputs generated by the distribution of network parameters approximates the distribution of observed elongation data. More formally, if the vector  $\lambda$  describes the network inputs reflecting the experimental conditions (light conditions and inactivated genes),  $g(\theta, \lambda)$  is the vector of network outputs for inputs  $\lambda$  and parameter  $\theta$  and  $\Omega$  is the (multi-dimensional) distribution of observed elongations in the conditions corresponding to  $\lambda$ , then the parameter space is sampled according to

$$p(\theta) \propto p_{\Omega}(g(\theta, \lambda))$$

This way, not only the average of observed elongations is taken into account, but also their variability, which also provides additional useful information. Sampling is done using GaA-MCMC<sup>(30)</sup>, resulting in a distribution for the parameter vector  $\theta$ . This distribution can then be used to make predictions for a new experimental condition by looking at the corresponding distribution of the network output for this new input. The mean of this distribution is estimated

and used as prediction value.

In order to evaluate a network, a leave-one-mutant-out procedure is followed, whereby the data for all genotypes but one mutant is used to train the parameters (i.e., estimate the distribution of  $\theta$ ) and predict the remaining mutant. This prediction is then compared to the actual observations for that mutant. This is done ten times for each mutant to evaluate the robustness of the prediction to random sampling effects. The network score is defined by the average Mahalanobis distance between the observed elongations and the predicted ones.

The model is implemented in C++ and the code is freely available under a GPL license on [www.unil.ch/cbg](http://www.unil.ch/cbg). It uses the CVODE library (31) as numerical equation solver. The sampling GaA-MCMC algorithm is implemented in matlab and provided by (30). Generating the simulation data presented in Fig 2 takes about two days on 30 CPUs (2.27 GHz, 256 GB RAM).

## Acknowledgments

We thank Laure Allenbach and Roger Granbom for technical support as well as Patricia Hornitschek and Markus Kohlen for starting the crosses with the *sav3* mutant, Anupama Goyal and Markus Kohlen for setting up the protocol to extract RNA from dissected seedlings, Ioannis Xenarios for fruitful discussions, Hiroshi Nozaki and Tomokazu Koshiba for generously providing Peo-IAA and yucasin, Joanne Chory for the *sav3-2* mutant, Ted Farmer, Niko Geldner, Sam Zeeman and Tim Hohm for critically reading the paper and Miguel Giraldo for the metaphorical illustration (Fig. S10). This work was supported by the University of Lausanne, a grant from SystemsX.ch “Plant Growth in a changing Environment” to C.F. and S.B., the Swedish Governmental Agency for Innovation Systems (VINNOVA) and the Swedish Research Council (VR) to K.L.

## References

1. Kami C, Lorrain S, Hornitschek P, Fankhauser C (2010) in *Current Topics in Developmental Biology*, pp 29–66.. 2010/08/14 Ed.
2. Casal JJ (2013) Photoreceptor signaling networks in plant responses to shade. *Annu Rev Plant Biol* 64:403–27.
3. Hautier Y, Niklaus P a, Hector A (2009) Competition for light causes plant biodiversity loss after eutrophication. *Science (80- )* 324:636–8.
4. Ballaré CL, Mazza C a, Austin AT, Pierik R (2012) Canopy light and plant health. *Plant Physiol* 160:145–55.
5. Yanovsky MJ, Casal JJ, Whitelam GC (1995) Phytochrome A, phytochrome B and HY4 are involved in hypocotyl growth responses to natural radiation in Arabidopsis: weak de-etiolation of the phyA mutant under dense canopy. *Plant, Cell Environ* 18:788–794.
6. Keller MM et al. (2011) Cryptochrome 1 and phytochrome B control shade-avoidance responses in Arabidopsis via partially independent hormonal cascades. *Plant J* 67:195–207.

7. Lorrain S et al. (2008) Phytochrome-mediated inhibition of shade avoidance involves degradation of growth-promoting bHLH transcription factors. *Plant J* 53:312–23.
8. Hornitschek P et al. (2012) Phytochrome interacting factors 4 and 5 control seedling growth in changing light conditions by directly controlling auxin signaling. *Plant J* 71:699–711.
9. Li L et al. (2012) Linking photoreceptor excitation to changes in plant architecture. *Genes Dev* 26:785–90.
10. Hornitschek P, Lorrain S, Zoete V, Michielin O, Fankhauser C (2009) Inhibition of the shade avoidance response by formation of non-DNA binding bHLH heterodimers. *EMBO J* 28:3893–902.
11. Sessa G et al. (2005) A dynamic balance between gene activation and repression regulates the shade avoidance response in Arabidopsis. *Genes Dev* 19:2811–2815.
12. Tao Y et al. (2008) Rapid synthesis of auxin via a new tryptophan-dependent pathway is required for shade avoidance in plants. *Cell* 133:164–76.
13. Keuskamp DH, Pollmann S, Voesenek LACJ, Peeters AJM, Pierik R (2010) Auxin transport through PIN-FORMED 3 (PIN3) controls shade avoidance and fitness during competition. *Proc Natl Acad Sci U S A* 107:22740–4.
14. Middleton AM, Farcot E, Owen MR, Vernoux T (2012) Modeling regulatory networks to understand plant development: small is beautiful. *Plant Cell* 24:3876–91.
15. He W et al. (2011) A small-molecule screen identifies L-kynurenine as a competitive inhibitor of TAA1/TAR activity in ethylene-directed auxin biosynthesis and root growth in Arabidopsis. *Plant Cell* 23:3944–60.
16. Won C et al. (2011) Conversion of tryptophan to indole-3-acetic acid by TRYPTOPHAN AMINOTRANSFERASES OF ARABIDOPSIS and YUCCAs in Arabidopsis. *Proc Natl Acad Sci U S A* 108:18518–23.
17. Nishimura T et al. (2013) Yucasin is a potent inhibitor of YUCCA, a key enzyme in auxin biosynthesis. *Plant J*:352–366.
18. Lilley JLS, Gee CW, Sairanen I, Ljung K, Nemhauser JL (2012) An endogenous carbon-sensing pathway triggers increased auxin flux and hypocotyl elongation. *Plant Physiol* 160:2261–70.
19. Sairanen I et al. (2012) Soluble carbohydrates regulate auxin biosynthesis via PIF proteins in Arabidopsis. *Plant Cell* 24:4907–16.

20. Wang R-S, Saadatpour A, Albert R (2012) Boolean modeling in systems biology: an overview of methodology and applications. *Phys Biol* 9:055001.
21. Mendoza L, Xenarios I (2006) A method for the generation of standardized qualitative dynamical systems of regulatory networks. *Theor Biol Med Model* 3:13.
22. Calderon-Villalobos LI, Tan X, Zheng N, Estelle M (2010) Auxin perception--structural insights. *Cold Spring Harb Perspect Biol* 2:a005546.
23. Calderón Villalobos LIA et al. (2012) A combinatorial TIR1/AFB-Aux/IAA co-receptor system for differential sensing of auxin. *Nat Chem Biol* 8:477–85.
24. Vert G, Walcher CL, Chory J, Nemhauser JL (2008) Integration of auxin and brassinosteroid pathways by Auxin Response Factor 2. *Proc Natl Acad Sci U S A* 105:9829–34.
25. Bergman RN (1989) Lilly lecture 1989. Toward physiological understanding of glucose tolerance. Minimal-model approach. *Diabetes* 38:1512–27.
26. Shannon CE (1948) A mathematical theory of communication. *Bell Syst Tech J* 27:379–423.
27. Laughlin SB, de Ruyter van Steveninck RR, Anderson JC, Steveninck RRDR Van (1998) The metabolic cost of neural information. *Nat Neurosci* 1:36–41.
28. Uda S et al. (2013) Robustness and compensation of information transmission of signaling pathways. *Science (80- )* 341:558–61.
29. Dornbusch T et al. (2012) Measuring the diurnal pattern of leaf hyponasty and growth in Arabidopsis - a novel phenotyping approach using laser scanning. *Funct Plant Biol* 39:860.
30. Müller CL, Sbalzarini IF (2010) in *EEE Congress on Evolutionary Computation (CEC)*.
31. Cohen SD, Hindmarsh AC (1996) CVODE, a stiff/nonstiff ODE solver in C. *Comput Phys* 10:138–143.

## Figure legends

**Fig.1: Regulation of the Shade Avoidance Response.** (A) 8 day-old seedlings grown under high or low R:FR conditions. (B) Main components regulating the shade-avoidance responses (see main text). (C and D) Network model and equation used for modeling. Arrows are inhibitory (red), or positive (black).

**Fig 2: Observed and predicted elongation of seedlings grown in low light intensity in normal (white background) and low R:FR (shaded background).** Box-plots correspond to observed experimental data and color dots indicate elongations predicted by the model (10 non-deterministic predictions are made for each condition). A, B and C correspond to predictions of the same data (identical box-plots) by different models, indicated in the upper-right corner (colored dots change across panels). The mean prediction error is indicated in the upper-right corner.

**Fig. 3. HFR1 inhibits auxin production.** (A) Hypocotyl length of seedlings grown with or without the auxin transport inhibitor NPA under low light conditions (see material and methods for seedling growth conditions). Data are mean  $\pm$  2SE, n=23-29. (B) Relative hypocotyl elongation in low light and in low R:FR in presence of L-kynurenine, an inhibitor of auxin production. n=25-34, error bars=2SE. (C) Free auxin content in seedlings grown under low light conditions subjected to 1hr of high or low R:FR. Data are mean  $\pm$  SE (n=5). (D) Quantitative RT-PCR analysis of 2 genes participating in the auxin production pathway. Seedlings were collected after 4 days in constant high R:FR light followed by 3 days in low or high R:FR. Data are mean  $\pm$  SE, n=3.

**Fig. 4. Auxin sensitivity and production depends on the light intensity.** (A) Modeling suggests different networks for low and high light intensity (best score in red, p-values obtained by a t-test) (B) Free auxin content in seedlings grown under high or low light intensity subjected to 1h of low R:FR or kept in high R:FR as a control. Data are mean +/- SE (n=5). Low light intensity data already presented in (8). (C) Relative hypocotyl elongation of wild-type seedlings in low R:FR in presence of inhibitor of auxin synthesis (L-kynurenine) or perception (PEO-IAA). n= 22-32, error bars= 2SE. (\*) represents statistical difference (t-test, p<0.01). (D) *AFB1* expression in hypocotyls of 7 day-old wild type seedlings grown in high and low light intensity, high R:FR or subjected for 2 hours to low R:FR. In low R:FR, *AFB1* is more expressed in low than in high light (\*, t-test, p<0.05). Data are mean +/-2SE (n=3 x 40 seedlings). (E) *AFB1* expression in entire seedlings of 7 day-old seedlings grown in low light intensity, high R:FR and subjected to 2 or 4h of low R:FR. Data are mean +/-2SE (n=3 x 40 seedlings).

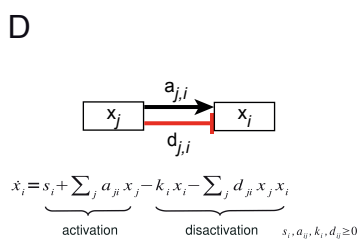
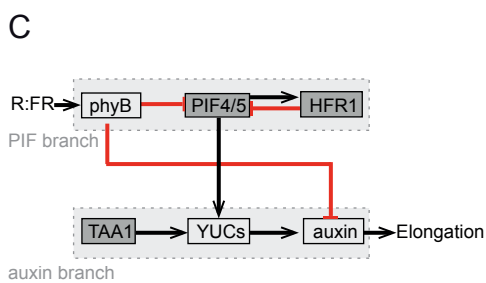
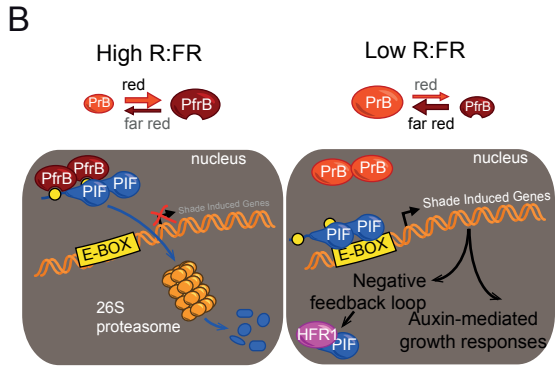
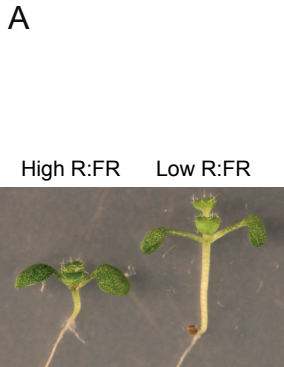


Figure 1

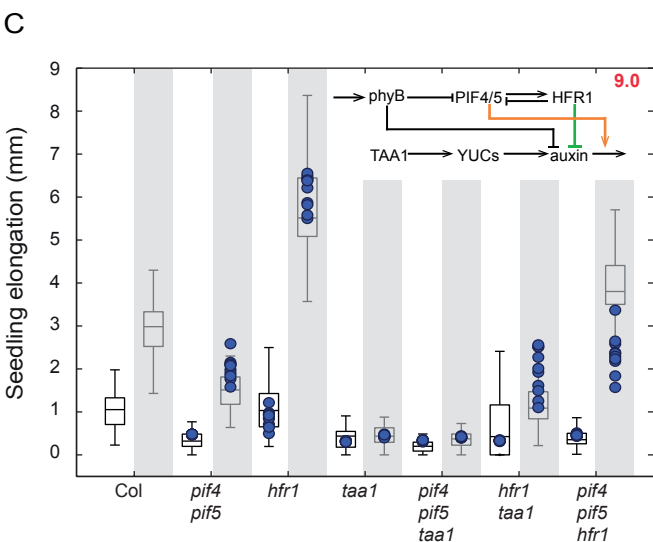
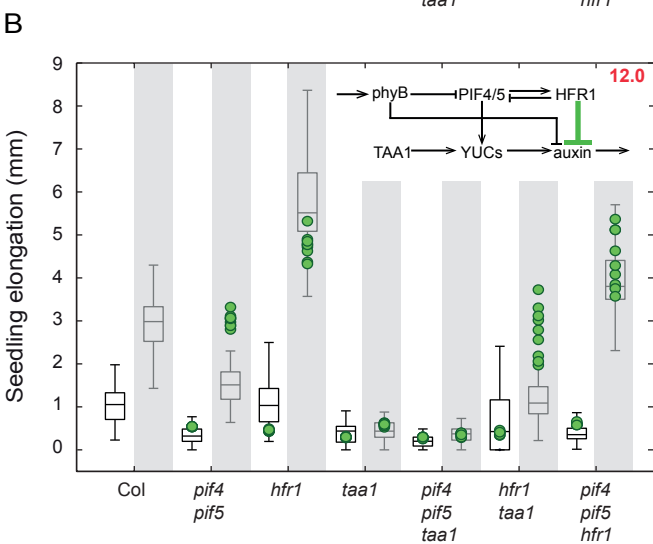
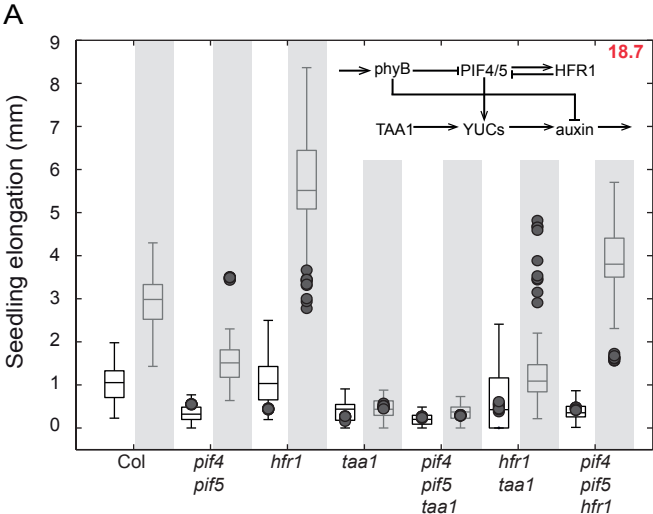


Figure 2

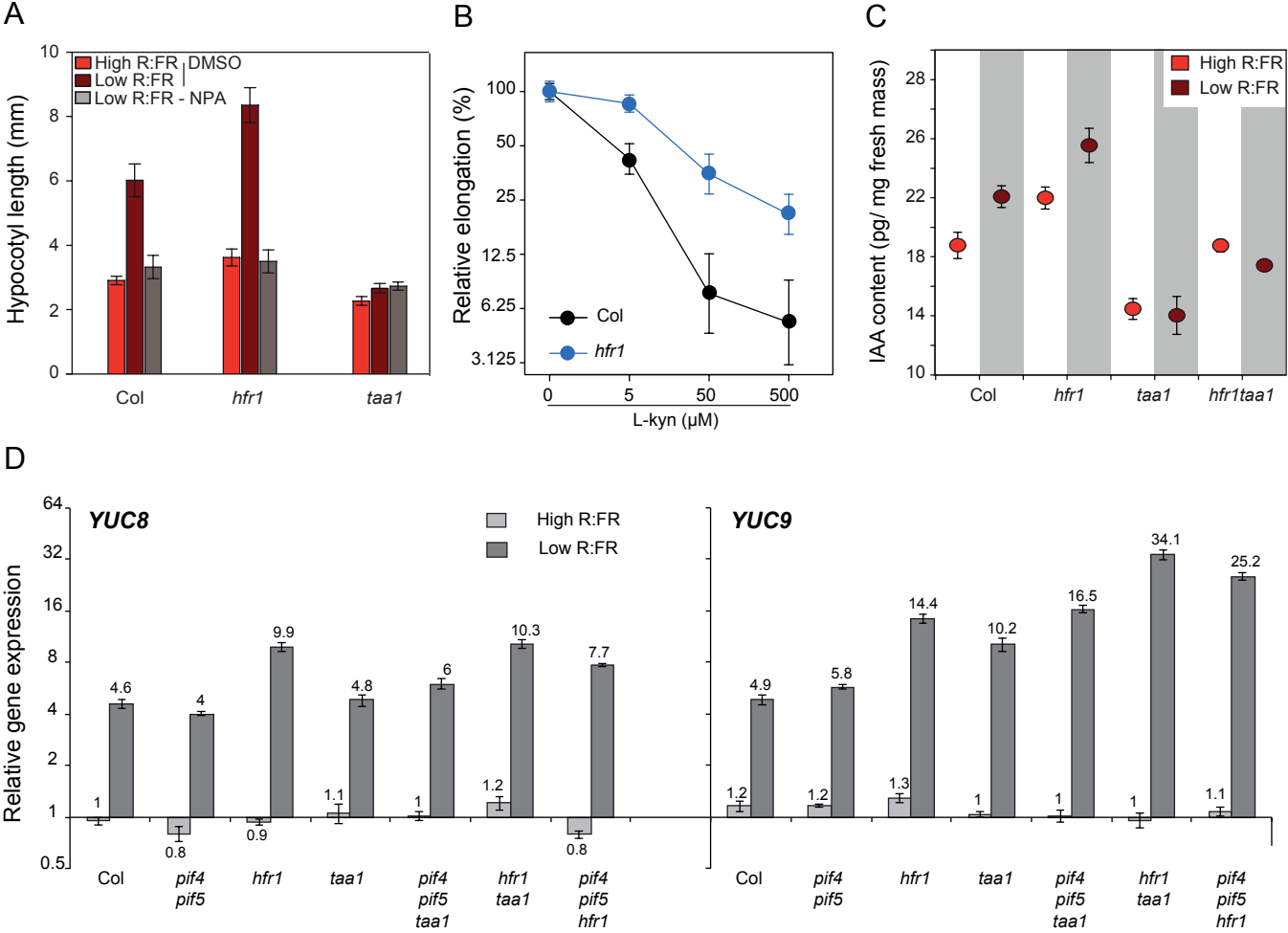
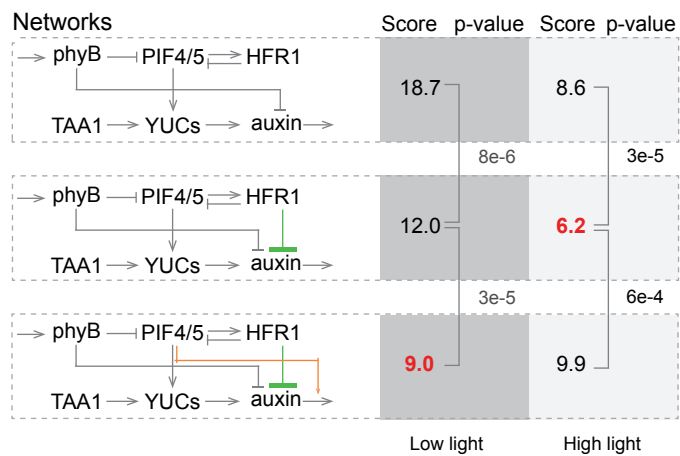
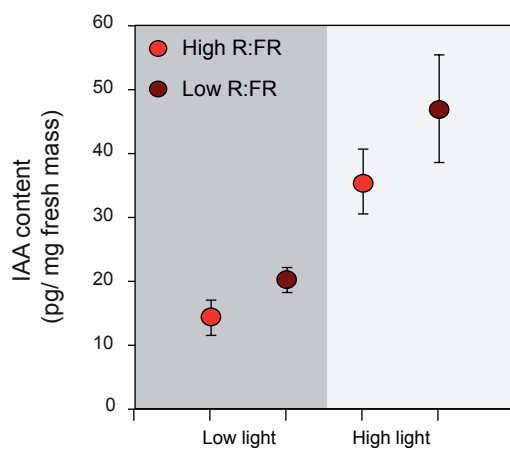


Figure 3

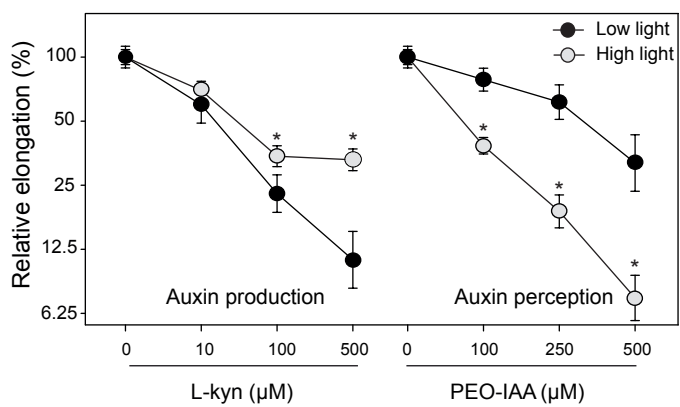
A



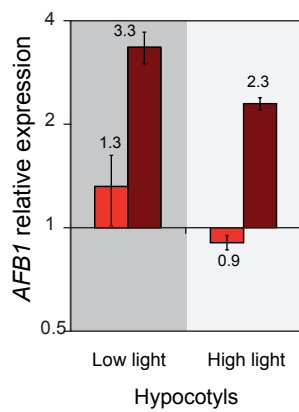
B



C



D



E

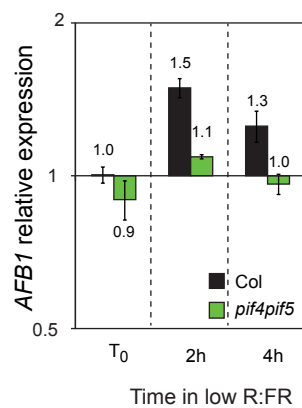


Figure 4

## Supplemental information

### Biological method

#### *Plant material*

All mutants were generated in the Col background. The *pif4pif5*, *hfr1*, *hfr1pif4pif5*, and *sav3-2/taal* mutants have been described previously by (1–3). The *hfr1taal* and *pif4pif5taal* mutants were obtained by crossing *sav3-2* respectively to *hfr1-101* and *pif4-101pif5* (*pil6-1*) and genotyping was performed as described in (1–3). For *sav3-2*, genomic DNA was amplified with CF505 (AACATCCCCATGTCCGATTT) and CF506 (AACACAAGTTCGTCATGTCGC). After digestion with *MnlI*, the WT fragment produces 2 bands of 220 and 108bp while the *sav3-2* is not digested.

#### *Pharmacological treatment*

For picloram (SIGMA-Aldrich)/PEO-IAA (provided by H. Nozaki)/L-kynurenine (SIGMA-Aldrich)/yucasin (provided by T. Koshiba) treatment, seedlings were first grown on ½ MS. After 4 days, the meshes were transferred on new ½ MS plates containing different concentrations of the drugs or DMSO as a control. All products were kept frozen as a 1000-time concentrated stock in DMSO. Hypocotyl elongation during the treatment was measured as the difference of hypocotyl length between day 4 and day 8 and expressed relative to the elongation of seedlings grown on DMSO.

#### *RNA extraction and RT-qPCR*

These experiments were performed as described in (4). For Real Time RT-PCR on dissected hypocotyls and cotyledons, 7-day-old seedlings grown on horizontal plates were harvested in cold acetone and vacuum infiltrated for fixation. Seedlings were moved to 70% Ethanol to dissect cotyledons and

hypocotyls. After removal of Ethanol samples were ground with glass beads and RNA was extracted using the RNeasy plant mini kit with on-column DNA digestion (Qiagen). 200 ng RNA was used for the reverse transcription as described in (8). Except when indicating in the figure legends, *YLS8* and *UBC10* were used as housekeeping genes.

#### *Determination of auxin content*

Aerial parts of seedlings were pooled, weighed, and frozen in liquid nitrogen for quantification of free IAA content. The sample fresh weight was around 10 mg, and five replicates were analyzed for each line and treatment. 500 pg  $^{13}\text{C}_6$ -IAA internal standard was added to each sample, and the samples were purified and analyzed using gas chromatography coupled to tandem mass spectrometry as described in (5), with minor modifications.

### **Computational methods**

#### *Model*

The regulatory network was modeled using ordinary differential equations. The same general purpose equation was used to model molecular activity. It is given by

$$\dot{x}_i = s_i + a_{ji}x_j - k_i x_i - d_{ji}x_j x_i \quad (1)$$

Here  $x_i$  represents the activity of node  $i$ , in our case the molecular activity and  $a_{ji}$  and  $d_{ji}$  are the weight of the positive and negative edges from node  $j$  to node  $i$  and are strictly positive. The positive source term  $s_i$  models all activating effects not explicitly represented in the network, such as baseline protein production. The degradation term  $k_i x_i$  models all inactivating effects not explicitly in the network. In this

equation, all effects are very coarsely approximated by a linear function, and the degradation term is bilinear. In sum, each positive edge corresponds to a linear activation, and each negative edge corresponds to a bilinear inhibition that ensures a positive activity. Relevant biological knowledge is also inserted in the model. For example, for mutants, the corresponding node activities are constrained to zero and the ratio of phyB activity in high versus low R:FR was set to 10, as documented by spectral measurements (6). Using contraction analysis (7), the system can be shown to converge to a single attractor as long as there is no cycle of positive edges in the network. The system is thus safely assumed to be at steady-state.. This set of equations differs from other general purpose network equations proposed in the literature, such as boolean network, continuous boolean networks (8) or Hopfield-like networks (9). In those networks, activities have a lower and upper bound (usually zero and one). Our network only has a lower bound but no upper bound. This, along with the use of linear activation terms, reduces the non-linearity of the network, which is very advantageous for the performance of the sampling algorithm we subsequently use. It can be justified on a theoretically level by assuming that molecular activities do not reach saturation level. Indeed, there can be differences of many orders of magnitude in the concentrations of proteins and assigning a gating function to the activities is also somewhat arbitrary, especially as units are left unspecified. Only for the readout node, hypocotyl elongation, we add a bounding sigmoidal function as we know that the observed elongations belong to the same order of magnitude. The sigmoidal function takes the following form

$$y = \beta(1 + \exp(-x + \beta/2))^{-1}$$

where  $\beta$  gives the amplitude (or saturation level) of the function, which has  $\beta/2$  as a fixed point.

We define the network parameter vector  $\theta$  consisting of the weight of all edges, the source and degradation terms of all nodes and  $\beta$ . Moreover, we set the list of experimental conditions  $\lambda$  as the (discrete) inputs of the network specifying the combinations of light conditions and the mutant used. We can then define the output vector  $g(\theta, \lambda)$  as the values of the elongation at steady state when using parameter values  $\theta$  and all experimental conditions  $\lambda$ . So for each parameter vector  $\theta$ , there is a vector of

outcomes  $g(\theta, \lambda)$ , specifying the values of the read-out node at steady state for each experimental condition in  $\lambda$ . These steady states are computed numerically.

The advantage of this model lies in its simplicity, as it only contains one effective parameter per node ( $s_i / k_i$ ) and one parameter per edge. In the present study, the network topology is also kept as simple as possible. If needed however the role of additional players can be explored since both node and edges can be expanded into more detailed sub-networks as long as we can generate enough data to constrain it with the relevant mutant combinations.

As mentioned above, this model cannot model sensitivity as activations are linear. When needed, we modeled the influence of node  $j$  on the sensitivity of node  $i$  to node  $k$  with a bilinear term  $a_{ijk} x_j x_k$ .

#### *Parameter sampling versus estimation*

In the method suggested here, a parameter sampling strategy rather than a parameter estimation strategy is applied. The idea behind it is to go beyond the “average response” criticized by Trewavas (10) and consider the distribution of the experimentally observed responses. Indeed, biological replicates differ one from another because each individual is to some extent unique, and this uniqueness can be related to the model parameters. One could argue that each biological replicate has a somewhat different parameter vector. So instead of considering an average response and estimating a vector of optimal parameters, as is commonly done, we sample the parameter space according to a particular distribution that depends on the distribution of the experimental data. Let  $\Omega$  be this  $m$ -dimensional experimental read-out distribution, where  $m$  is the number of different conditions and genotypes (i.e., the size of  $\lambda$ ). In other words,  $\Omega$  is the distribution of measured hypocotyl elongations, where each mutant and experimental condition runs along a different dimension. Since the conditions are independent, this distribution is assumed to be Gaussian with diagonal covariance matrix. Using a Markov Chain Monte Carlo method, GaA-MCMC (11), we then sample a parameter vector  $\theta$  according to

$$p(\theta) \propto p_{\Omega}(g(\theta, \lambda))$$

In other words,  $\theta$  is sampled such that the distribution of the corresponding network outcomes  $g(\theta, \lambda)$  follows  $\Omega$ , the experimental distribution of the hypocotyl elongation. This means that each point  $\theta$  of the parameter space is (theoretically) assigned a probability and this probability corresponds to the probability of observing  $g(\theta, \lambda)$  according to  $\Omega$ . The distribution  $p(\theta)$  captures our uncertainty of the parameter values as we do not settle for a single parameter vector, but assign a probability to the whole parameter space. This enables the exploitation of the information contained in the variance of the experimental data (both in terms of biological regulation and experimental uncertainties), and not only its average as done by classical parameter optimization. Having a distribution on the network parameters  $\theta$  allows us to predict the effect of a new knock-out mutant by solving the network equation at steady-state for each of the sampled parameters and looking at the distribution of responses. The mean of the resulting response provides a prediction and its variance gives a measure of confidence in this prediction.

This approach is similar to the Approximate Bayesian Computation (ABC) methods often used for stochastic models in population genetics (12), and which have also been applied to model selection (13). Those methods also sample the parameter space for example with MCMC (14) and the probabilistic (or varying) outcome of the model for each parameter  $\theta$  is compared to the distribution of the observed data. This is done to estimate the posterior likelihood function of  $\theta$ , which can then be maximized. In contrast, in our case, each parameter  $\theta$  generates a single output and the distribution of  $\theta$  in the biological samples is estimated by matching the distribution of corresponding model outcome to distribution of the observations. In this sense, it can hardly be said to be a Bayesian likelihood function and the Bayes factor (essentially a likelihood ratio) cannot be used for model selection. Instead we use leave-one-out cross-validation, as described below.

### *Network evaluation*

In order to evaluate the network we look at the accuracy of its predictions in a leave-one-out cross-validation scheme. All but one mutant data are used to sample the parameter space (as described above)

and the resulting parameter distribution is then used to predict the elongation of the remaining mutant (called the test mutant). This prediction is done by estimating the mean of the distribution of elongations of the test mutant when sampling from the distribution of parameters. This is done for all mutants, providing a prediction for each mutant in normal and simulated shade conditions. The Mahalanobis distance between the predicted and the observed mean elongations are then used to quantify the accuracy of the predictions. This is equivalent to the absolute log z-score of the predictions according to the experimental distribution of elongations. It thus reflects how well the network can capture the essential features of the biological system. If the distance is zero, it means that all mean mutant elongations are perfectly predicted. The bigger the distance is, the poorer the predictions are (and thus the network). Since the sampling entails some randomness, we assess the reliability of the predictions and evaluation by running the evaluation procedure ten times and looking how much they vary from one another. The final score is the average score across the ten runs. This procedure penalizes overfitting, as can be seen from the simulation results where having both the sensitivity and production of the PIFs in the network does not produce a better score than having just one of them (see Fig 2C vs Fig. S2 and Fig. S5B vs Fig. S5C).

### *Noise model*

We consider the following simple elongation model,  $y_{lgi} = b_{lg} x_{lgi}$ , where  $y$  is the observed elongation,  $x$  is the auxin signal,  $b$  is the auxin sensitivity and  $l$ ,  $g$  and  $i$  denote respectively the light condition, the genotype and the seedling index. To model noise, we include a multiplicative noise  $\varepsilon$  and an additive measurement noise  $\mu$ , obtaining  $y_{lgi} = b_{lg} x_{lgi} \varepsilon_{lgi} + \mu_{lgi}$ . This model is justified by the fact that the standard deviation scales linearly with the average elongation (see Fig. ). We are interested in the variance of  $\varepsilon$ , which can be interpreted as the variance in the auxin signal read-out. Assuming noise independence,

we have  $\text{var}(\varepsilon_{lg}) = \frac{\text{var}(y_{lg}) - \text{var}(\mu_{lg})}{(b_{lg} x_{lg})^2}$ . We estimated the variance of measurement noise  $\text{var}(\mu_{lg})$

(assumed to be the same for all  $l$  and  $g$ ) by measuring twice the same data set, while  $b_{lg} x_{lg}$  is estimated as

the average elongation for a given light condition and genotype. Assuming normal distributions for  $\mu$  (centered) and  $\varepsilon$  (centered on 1), a F-test can be used to assess whether  $\text{var}(\varepsilon_{lg})$  varies significantly between two conditions.

### **List of Supplemental figures:**

Fig. S1: Experimental set-up.

Fig. S2: Observed and predicted elongation of seedlings grown in low light intensity in normal (white background) and low R:FR (shaded background) for the network including the link between PIF and auxin production (through the YUC ) and auxin sensitivity.

Fig. S3: Quantitative RT-PCR analysis of shade-responsive genes.

Fig. S4: Quantitative RT-PCR analysis of *YUC* genes in the *hfr1pif7* double mutant.

Fig. S5: Observed and predicted elongation of seedlings grown in high light intensity conditions.

Fig. S6: Differential effect of yucasin on *pif4pif5* depending on PAR.

Fig. S7: Hypocotyl elongation in response to low R:FR of *taa1*.

Fig. S8: *AFB1* expression is not induced in the cotyledons in response to low R:FR.

Fig. S9: noise analysis.

Fig. S10: Metaphorical illustration of the model.

## Supplemental figure legend

**Fig. S1: Experimental set-up.** (A) Seedlings were grown on vertical plates along a nylon mesh. Pictures were taken at day 4 and at day 8. (B) Hypocotyl elongation during the last 4 days of the experiment. Hypocotyl elongation during the treatment was measured as the difference of hypocotyl length between day 4 and day 8. n=25-34, error bars=2SE.

**Fig. S2: Observed and predicted elongation of seedlings grown in low light intensity in normal (white background) and low R:FR (shaded background) for the network including the link between PIF and auxin production (through the YUC ) and auxin sensitivity.**

**Fig. S3: Quantitative RT-PCR analysis of shade-responsive genes.** The different genotypes were grown 4 days in constant high R:FR light followed by 3 days in low or high R:FR. Gene expression was normalized to *YLS8* and *UBC* and expressed relative to one WT control grown under high R:FR. Error bars represent the standard error of the mean of three biological replicates.

**Fig. S4: Quantitative RT-PCR analysis of *YUC* genes in the *hfr1pif7* double mutant.** The different genotypes were grown 4 days in constant high R:FR light followed by 3 days in low or high R:FR. Gene expression was normalized to *YLS8* and *UBC* and expressed relative to one WT control grown under high R:FR. Error bars represent the standard error of the mean of three biological replicates.

**Fig. S5: Observed and predicted elongation of seedlings grown in high light intensity conditions.**

Network B makes predictions significantly better than all other networks. Refer to the legend of Fig. 2 and to Fig. 4A for more details.

**Fig. S6: Differential effect of yucasin on *pif4pif5* depending on PAR.** Relative hypocotyl elongation of wild-type seedlings in low R:FR in presence of inhibitor of auxin synthesis (yucasin) at the concentration of 100 $\mu$ M.  $n > 14$ , mean  $\pm 2$ SE, (\*) represents statistical difference ( $p < 0.01$ ) using a t-test. As previously published (15), the efficiency of yucasin to inhibit hypocotyl elongation is limited.

**Fig. S7: Hypocotyl elongation in response to low R:FR of *taa1*.** (A) Hypocotyl length of seedlings grown in high or low R:FR under low or high light conditions.  $n = 23-30$ , error bars = 2SE. (B) Hypocotyl length of 8 day-old seedlings grown under high or low R:FR, high intensity in presence of inhibitor of auxin perception (PEO-IAA). Experiments were conducted as described in Fig. 2B.

**Fig. S8: *AFBI* expression is not induced in the cotyledons in response to low R:FR.**

Gene expression was determined by RT-qPCR in cotyledons of 7 day-old wild type seedlings grown in low light intensity, high R:FR (T0) or subjected for 2 hours to low R:FR (2h). Data are mean  $\pm 2$ SE ( $n = 3 \times 40$  seedlings).

**Fig. S9: Noise analysis.** For most genotypes and conditions, a linear relationship is observed between mean elongation and its standard deviation, confirming the validity of an additive and multiplicative noise model. In high light, the Col elongation displays less variability than what would be expected from its

mean elongation, suggesting that the increased auxin signal intensity makes it more robust. Interestingly, this is not the case for the *pif4pif5* mutants. The regression line for low light conditions is shown in blue.

**Fig. S10: Metaphorical illustration of the model.** In foliar shade, a weaker signal (represented by fewer auxin molecules) is compensated by an increased sensitivity (represented by the hearing aid)

## References

1. Lorrain S et al. (2008) Phytochrome-mediated inhibition of shade avoidance involves degradation of growth-promoting bHLH transcription factors. *Plant J* 53:312–23.
2. Tao Y et al. (2008) Rapid synthesis of auxin via a new tryptophan-dependent pathway is required for shade avoidance in plants. *Cell* 133:164–76.
3. Hornitschek P, Lorrain S, Zoete V, Michielin O, Fankhauser C (2009) Inhibition of the shade avoidance response by formation of non-DNA binding bHLH heterodimers. *EMBO J* 28:3893–902.
4. Hornitschek P et al. (2012) Phytochrome interacting factors 4 and 5 control seedling growth in changing light conditions by directly controlling auxin signaling. *Plant J* 71:699–711.
5. Andersen SU et al. (2008) Requirement of B2-type cyclin-dependent kinases for meristem integrity in *Arabidopsis thaliana*. *Plant Cell* 20:88–100.
6. Mancinelli A (1994) in *Photomorphogenesis In Plants-2nd edition*, eds Kendrick RE, Kronenberg. GHM (Springer), pp 211–269.
7. Lohmiller W, Slotine J-JE (1998) On Contraction Analysis for Non-linear Systems. *Automatica* 34:683–696.
8. Mendoza L, Xenarios I (2006) A method for the generation of standardized qualitative dynamical systems of regulatory networks. *Theor Biol Med Model* 3:13.
9. Ciliberti S, Martin OC, Wagner a. (2007) Innovation and robustness in complex regulatory gene networks. *Proc Natl Acad Sci U S A* 104:13591–6.
10. Trewavas A (2003) Aspects of plant intelligence. *Ann Bot* 92:1–20.
11. Müller CL, Sbalzarini IF (2010) in *EEE Congress on Evolutionary Computation (CEC)*.

12. Marin J-M, Pudlo P, Robert CP, Ryder R (2011) Approximate Bayesian Computational methods. *Stat Comput* 22:1167–1180.
13. Toni T, Stumpf MPH (2010) Simulation-based model selection for dynamical systems in systems and population biology. *Bioinformatics* 26:104–10.
14. Marjoram P, Molitor J, Plagnol V, Tavaré S (2003) Markov chain Monte Carlo without likelihoods. *Proc Natl Acad Sci U S A* 100:15324–8.
15. Nishimura T et al. (2013) Yucasin is a potent inhibitor of YUCCA, a key enzyme in auxin biosynthesis. *Plant J*:352–366.

Figure S1

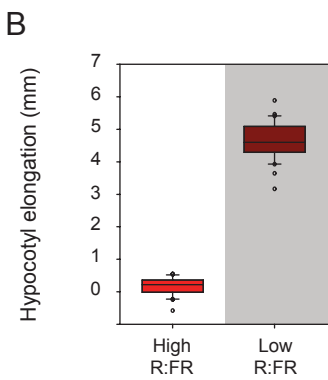
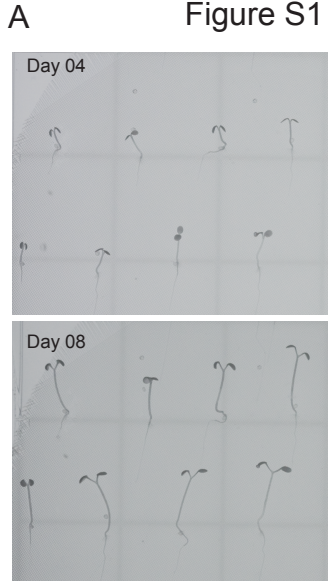


Figure S2

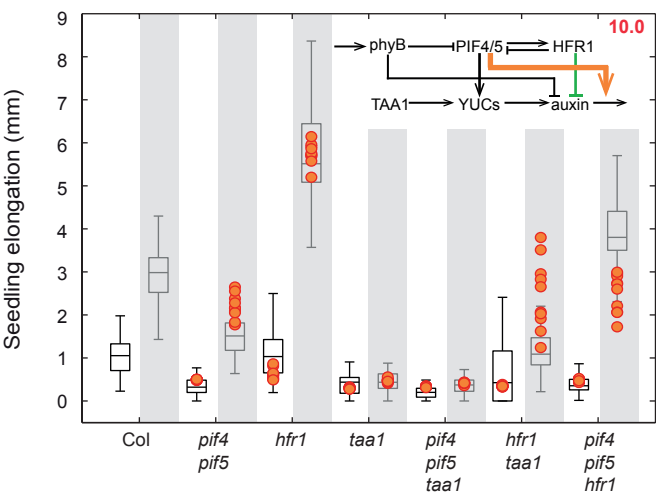


Figure S3

High R:FR  
Low R:FR

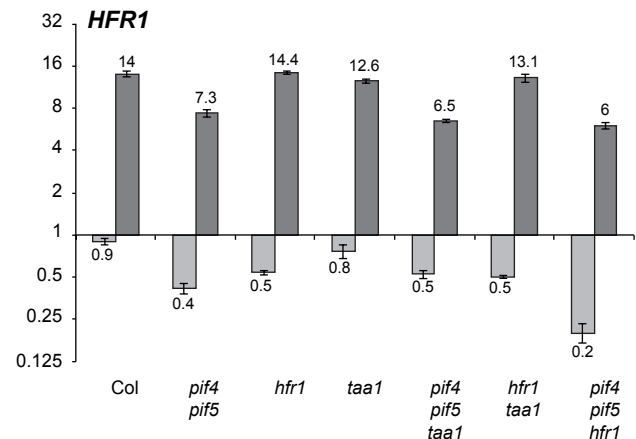
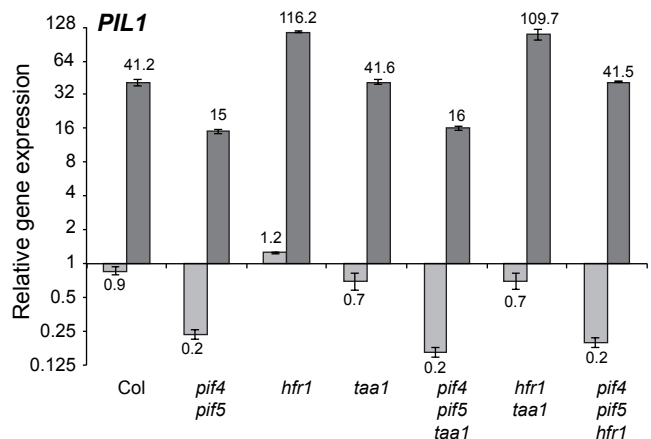
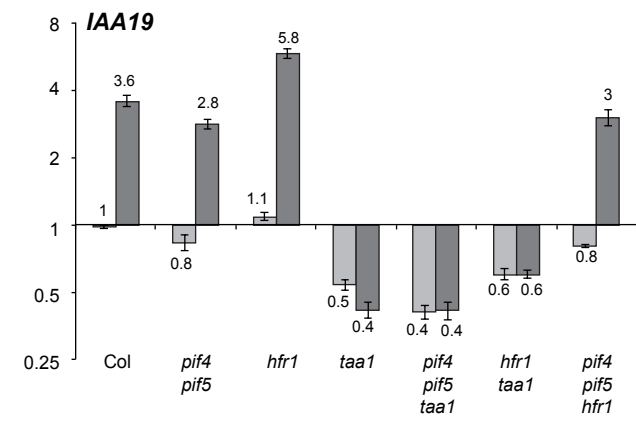
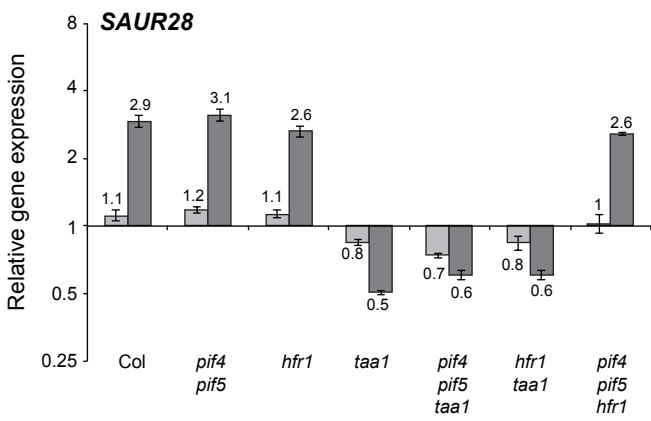
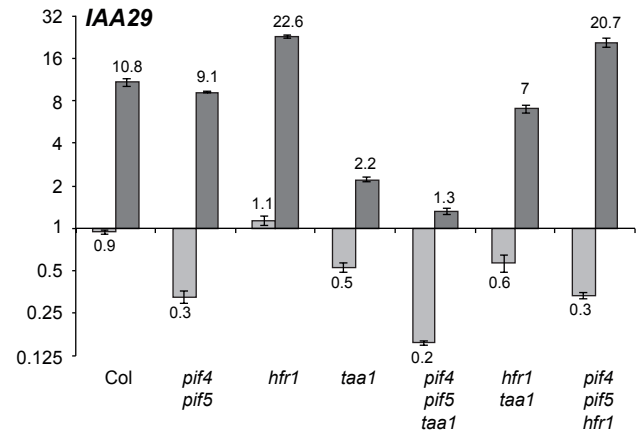
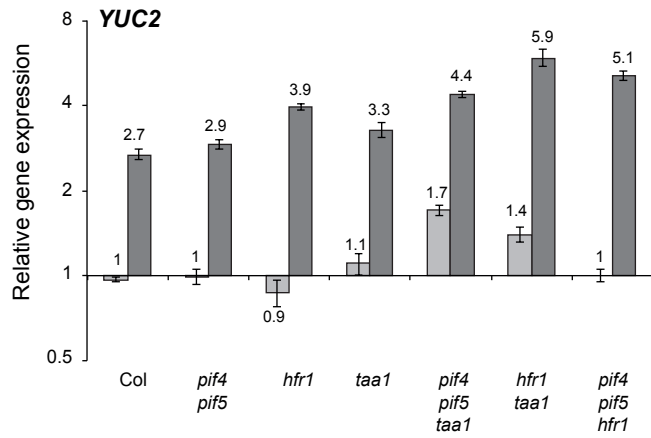


Figure S4

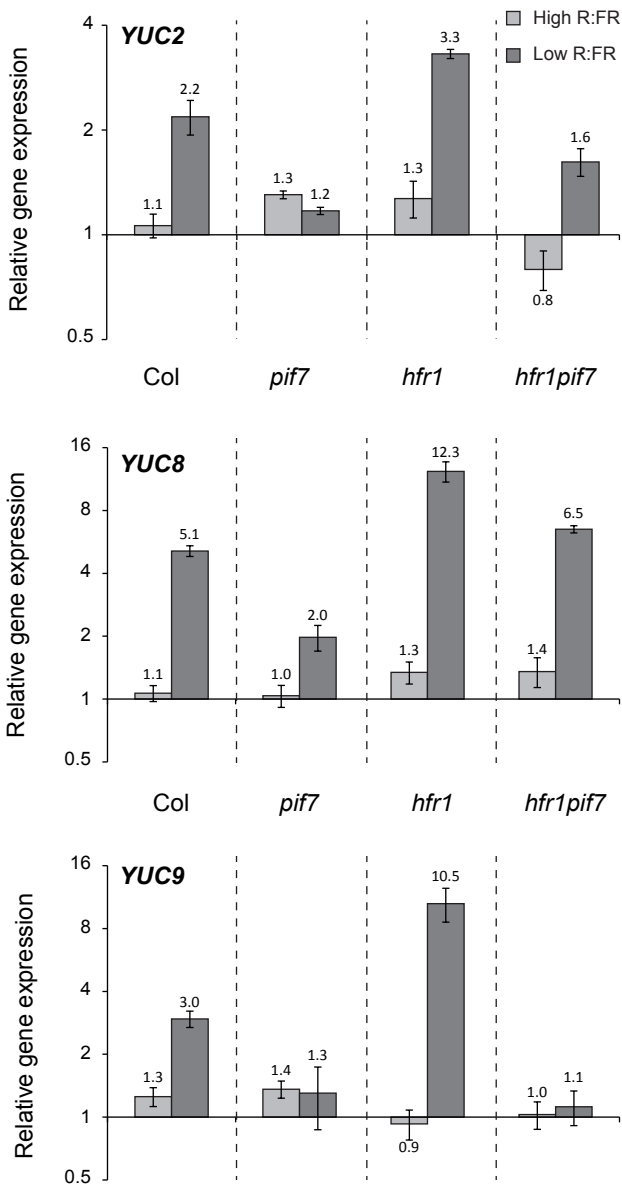


Figure S5

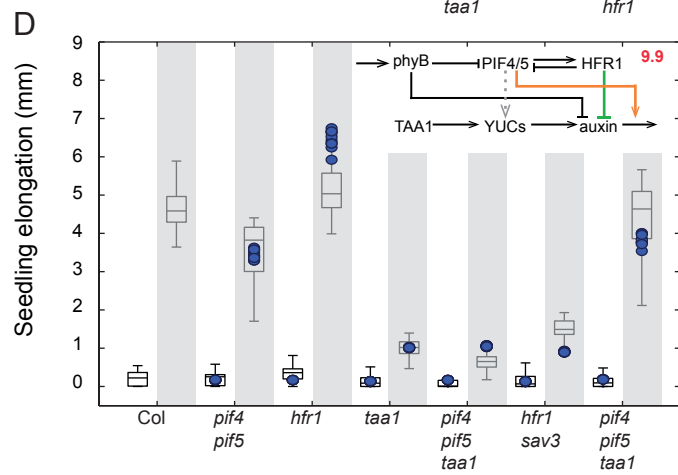
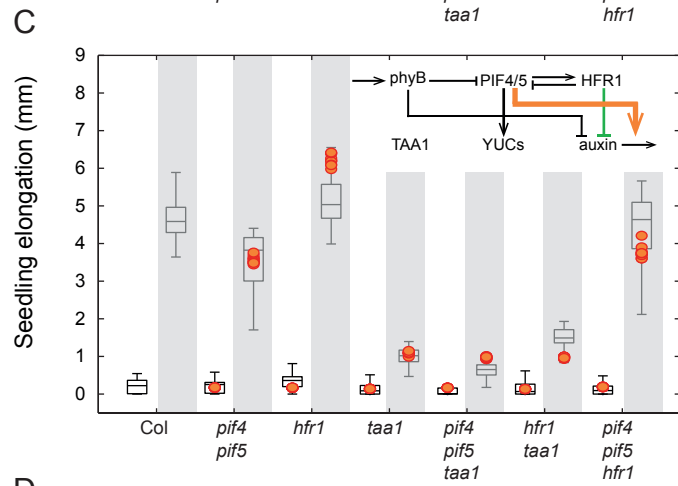
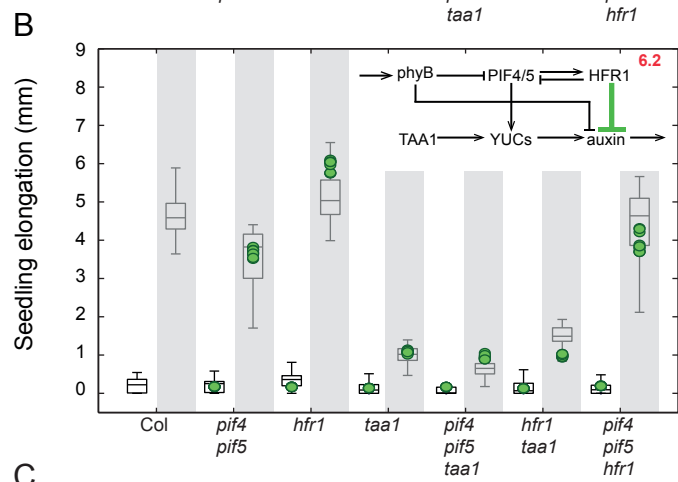
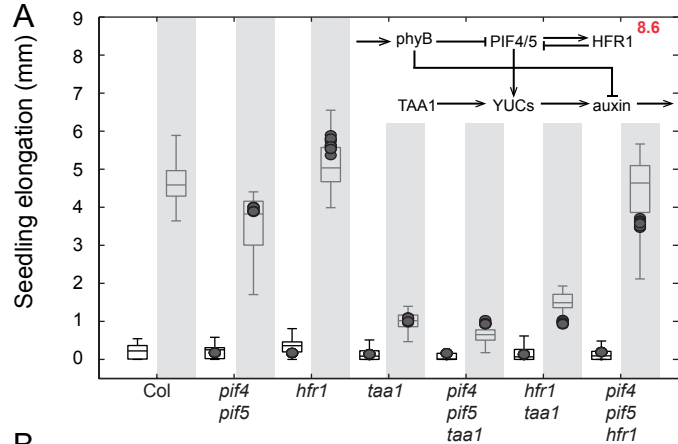


Figure S6

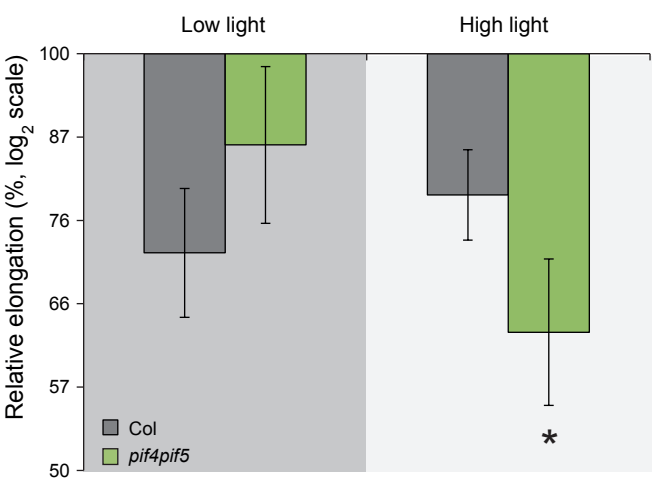
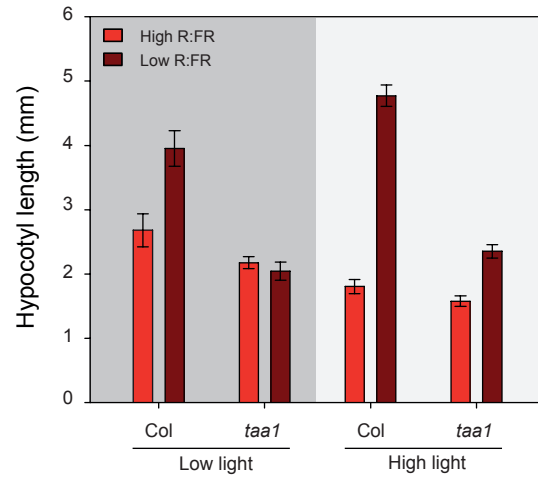


Figure S7

A



B

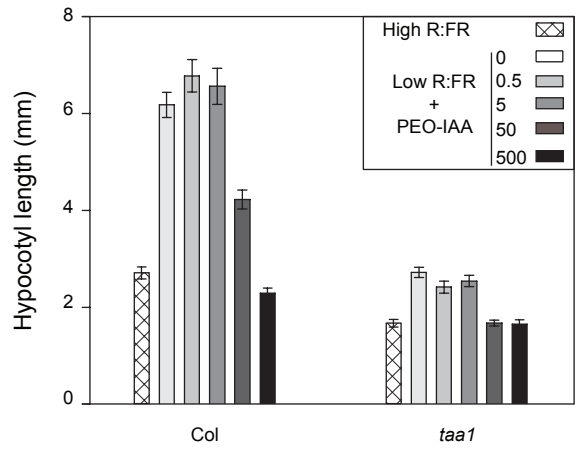


Figure S8

Cotyledons

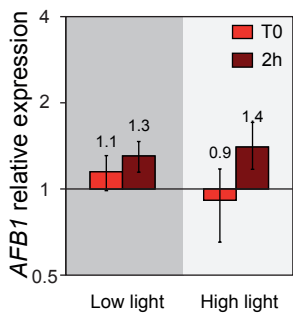


Figure S9

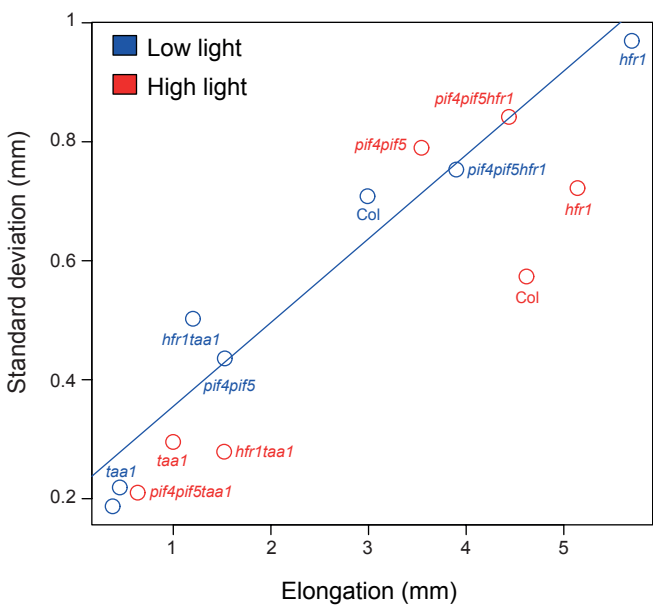


Figure S10

